Oxid Met (2014) 82:359–381
DOI 10.1007/s11085-014-9496-1

ORIGINAL PAPER

Long-Term Oxidation of Candidate Cast Iron and Stainless Steel Exhaust System Alloys from 650 to 800 °C in Air with Water Vapor

M. P. Brady · G. Muralidharan · D. N. Leonard · J. A. Haynes · R. G. Weldon · R. D. England

Received: 23 May 2014 / Revised: 4 August 2014 / Published online: 29 August 2014

Abstract The oxidation behavior of candidate cast irons and cast stainless steels for diesel exhaust systems was studied for 5,000 h at 650–800 °C in air with 10 % H_2O. At 650 °C, Ni-resist D5S exhibited moderately better oxidation resistance than did the SiMo cast iron. However, the D5S suffered from oxide scale spallation at 700 °C, whereas the oxide scales formed on SiMo cast iron remained relatively adherent from 700 to 800 °C. The oxidation of the cast chromia-forming austenitics trended with the level of Cr and Ni additions, with small mass losses consistent with Cr oxy-hydroxide volatilization for the higher 25Cr/20–35Ni HK and HP type alloys, and transition to rapid Fe-base oxide formation and scale spallation in the lower 19Cr/12Ni CF8C plus alloy. In contrast, small positive mass changes consistent with protective alumina scale formation were observed for the cast AFA alloy under all conditions studied. Implications of these findings for exhaust system components are discussed.

Keywords Water vapor · Exhaust · Cast iron · Austenitic · Oxidation

Introduction

Silicon–molybdenum (SiMo) cast irons are widely used for exhaust components, such as manifolds and turbocharger housings, in automotive and heavy duty truck diesel engine applications [1–6]. Increased operating temperatures and improved thermal management are expected to enable significant increases in power density,

M. P. Brady (✉) · G. Muralidharan · D. N. Leonard · J. A. Haynes
Oak Ridge National Laboratory, Oak Ridge, TN 37831-6115, USA
e-mail: bradymp@ornl.gov

R. G. Weldon · R. D. England
Cummins Inc., Box 3005, Columbus, IN 47202-3005, USA

offering the potential for greater power output for the same sized engine or engine downsizing (light weighting) for the same power output to achieve higher efficiencies and better mileage. However, the increased operating temperatures needed are expected to push SiMo cast iron properties such as strength, fatigue, and oxidation beyond their acceptable limits. This has resulted in increased interest in advanced cast irons, as well as cast ferritic and austenitic alloys with better oxidation resistance for next generation, higher temperature exhaust components.

A number of studies of the high temperature oxidation behavior of SiMo cast irons, in some cases in comparison to advanced cast irons, cast ferritics, and/or cast austenitics, under conditions relevant to exhaust systems have recently been reported [3–12]. However, these studies have focused on mechanistic aspects and characterization after relatively short term oxidation exposures (generally <500 h). The goal of the present work was to complement the existing literature by investigating the long-term oxidation resistance (5,000 h total) of a series of candidate next generation exhaust component alloys relative to SiMo cast iron in the temperature range of 650–800 °C. The exposures were conducted in an aggressive laboratory test condition of air with 10 vol% water vapor, as exhaust gases contain water vapor (typically 2–12 % for diesel exhaust [13], and water vapor is frequently linked with significant degradation in oxidation resistance, particularly for Cr-containing alloys [14, 15].

Experimental Procedures

Eight alloys of interest for exhaust components were selected for study: a 4.1Si–0.7Mo–3.1C weight percent (wt%) nodular ferritic SiMo cast iron, a 35Ni–4.7Si–2Cr–1.4C nodular austenitic D5S cast iron (comparable coefficient thermal expansion, CTE, to SiMo), a 19Cr–12Ni austenitic CF8C plus (CF8CP) alloy [16–18], austenitic 25Cr/20Ni type cast HK and TMA 4705 [19–22] stainless steels, austenitic 25Cr/35Ni type cast HP and TMA 6301 stainless steels [19–22], and a developmental 14Cr–25Ni–3.5Al cast alumina-forming austenitic (CAFA) stainless steel alloy designated CAFA 4 [23, 24]. Analyzed compositions are presented in Table 1 (all compositions presented in wt%). The SiMo, D5S, HK, TMA 4705, HP, TMA 6301, and CF8CP were electro discharge machine (EDM) cut from commercial castings, and the CAFA 4 EDM cut from a 0.5 kg range laboratory vacuum arc-casting.

Oxidation test samples ~20 mm × 10 mm × (1–1.5) mm were polished to a 600 grit USA finish using SiC polishing papers. Oxidation exposures were conducted in 100 h cycles at 650, 700, 750, and 800 °C with mass changes measured after every cycle (air cooling). Oxidation in air with 10 vol% water vapor was conducted by flowing air through an alumina tube inside a resistively heated tube furnace [25]. Distilled water was added by atomization into the flowing gas stream above its condensation temperature. The tests at 650, 700, and 800 °C were conducted using flow rates of ~850 cc/min (air) and ~4.5–5.0 cc/h (water), with a furnace tube diameter of ~5.5 cm. The 750 °C test was conducted in a ~8.7 cm diameter furnace tube, with ~2,000 cc/min (air) and ~10 cc/h (water). Test

Table 1 Alloy compositions (balance Fe) in wt% measured by inductively coupled plasma and combustion techniques

Alloy	Ni	Cr	Mo	Si	Al	Mn	Nb	V	W	Ti	Co	C	N	S	Other
SiMo	0.01	0.02	0.7	4.1	0.01	0.24	–	–	–	0.04	–	3.13	32	40	0.02Cu 0.03 Mg 0.015P
D5S	34.69	1.96	0.68	4.69	0.01	0.38	–	–	–	–	–	1.39	42	50	0.01Cu 0.03 Mg 0.017P
CF8CP	12.50	19.27	0.35	0.45		3.43	0.83	0.07	0.02		0.09	0.075	2,420	40	0.41Cu 0.02P
HK	18.14	25.57	0.05	1.68		0.93	0.19	0.02	0.07		0.07	0.47	490	70	0.06Cu 0.02P 0.01Ta
TMA 4705	20.81	25.91	0.18	1.5	–	0.66	0.38	0.04	0.28	–	1.16	0.7	420	70	0.01Cu 0.01P
HP	34.17	25.48	0.04	1.61		0.63	1.14	0.04	0.24		0.1	0.42	611	30	0.05Cu 0.02P 0.001B
TMA 6301	34.17	25.75	0.06	1.23	–	0.96	0.43	0.04	0.42	0.06	0.07	0.44	570	50	0.06Cu 0.022P
CAFA 4	25.28	14.11	1.98	0.48	3.49	1.92	0.94	0.05	1.00	0.05	–	0.29	12	13	0.008B 0.51Cu 0.02P

N and S reported in weight parts per million (wppm). Composition data for CAFA 4 from Ref. 24

samples were positioned in alumina boats in the furnace hot zone so as to expose the specimen faces parallel to the flowing gas. It should be noted that the 800 °C air with 10 % H_2O oxidation mass change data for CAFA 4, HP, and HK were previously reported in Ref. [24], and are included in the present work for comparison purposes. For most alloys and temperature conditions duplicate samples were run, typically one for 1,000 h and the second for 5,000 h. Unless otherwise specified, the mass change data shown is for the 5,000 h samples and the 1,000 h mass change data was of similar values to the first 1,000 h of the 5,000 h data.

For the SiMo cast iron and D5S material, additional oxidation data was obtained in 500 h cycles at 650 and 700 °C open to laboratory air (~50 % daily humidity, no added water vapor, referred to as "dry air" for convenience). These dry air samples were exposed in individual crucibles with lids, so it was possible to track both sample mass change and total sample mass change and spall. Selected oxidized samples were cross-sectioned and analyzed by optical microscopy, scanning electron microscopy (SEM) with energy dispersive X-ray analysis (EDS), and quantitative electron probe microanalysis (EPMA) using pure element standards for the metallic components.

Results

Oxidation Kinetics

Oxidation data in the temperature range of 650–800 °C in air with 10 % H_2O are shown in Figs. 1, 2, 3 and 4. The SiMo and D5S cast irons exhibited several orders of magnitude faster oxidation than the chromia- and alumina-forming austenitics under all conditions studied. Such behavior is expected, and consistent with their very low Cr contents and dependence on modest levels of Si for oxidation resistance (Table 1). At 650 °C in air with 10 % H_2O, the D5S exhibited moderately lower oxidation kinetics than the SiMo cast iron (Fig. 1), with mass change of ~50 mg/cm^2 for SiMo and ~30 mg/cm^2 for D5S after 5,000 h and little to no oxide scale spallation evident. However, at 700 and 750 °C in air with 10 % H_2O, the D5S suffered from oxide scale spallation and mass loss in the first few hundred hours of exposure, whereas the oxide scale formed on the SiMo cast iron remained adherent despite specific mass gains (mass change normalized by initial, unoxidized sample surface area; referred to only as "mass change" in remainder of text for simplicity) of nearly 100 mg/cm^2 at 700 °C. Because of this susceptibility to oxide scale spallation, the D5S was not evaluated at 800 °C.

The SiMo cast iron exhibited an unusual pattern of oxidation mass change behavior with increasing temperature. The extent of oxidation increased from 650 to 700 °C, with mass change of ~50 mg/cm^2 after 5,000 h at 650 °C and ~90 mg/cm^2 at 700 °C (Figs. 1, 2). However, the extent of oxidation for SiMo at 750 °C in air with 10 % H_2O (Fig. 3) was lower than at 700 °C, with mass change of only ~50 mg/cm^2 after 5,000 h. At 800 °C in air with 10 % H_2O (Fig. 4), the oxidation of SiMo was significantly lower up to 3,000 h of exposure (~20 mg/cm^2 at 3,000 h), at which point the oxidation increased, with mass change of

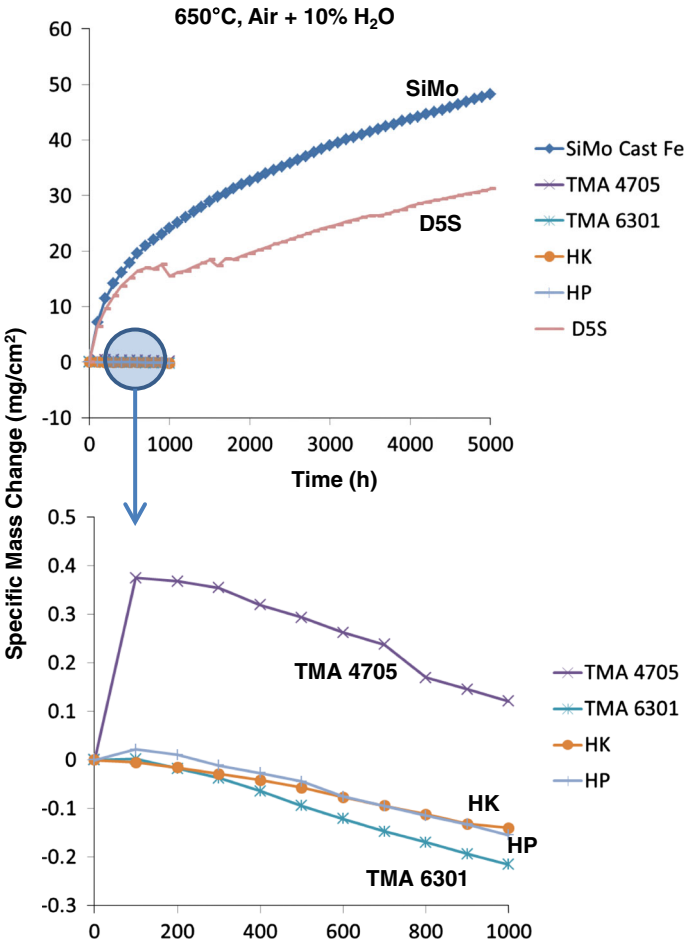

Fig. 1 Oxidation data (100 h cycles) at 650 °C in air with 10 % H_2O. Same data, two different specific mass change scales

$\sim$100 mg/cm^2 at 5,000 h. No significant mass loss or scale spallation was observed for the SiMo under all conditions studied.

The pattern of oxidation behavior for the chromia-forming austenitics trended with the level of Cr and Ni additions in these alloys. At 800 °C in air with 10 % H_2O (Fig. 4), the lowest Cr and Ni alloy, CF8CP with $\sim$19Cr and $\sim$12Ni (Table 1), exhibited extensive mass loss and scale spallation (~ -60 mg/cm^2 at 2,000 h of exposure) consistent with rapid, nonadherent Fe-oxide base scale formation. In contrast, good oxidation resistance with only modest mass loss behavior (0 to -1 mg/cm^2 range) consistent with chromia volatilization was observed for the first 2,500 h of exposure for the $\sim$20Ni–25Cr class HK and TMA 4705 alloys, and the $\sim$35Ni–25Cr HP and TMA 6301 alloys. The HK alloy

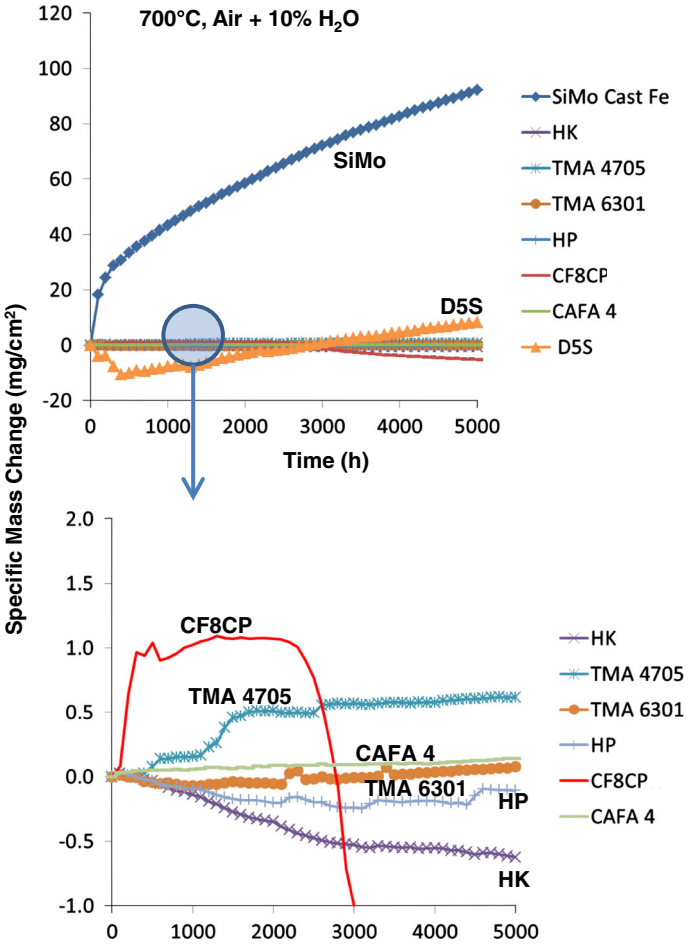

Fig. 2 Oxidation data (100 h cycles) at 700 °C in air with 10 % H_2O. Same data, two different specific mass change scales

exhibited a transition to Fe-oxide scale formation and spallation from ~2,500 to 5,000 h of exposure, whereas the TMA 4705, HP, and TMA 6301 continued to exhibit only modest mass loss behavior (all less than −3 mg/cm^2 after 5,000 h at 800 °C).

Modest mass loss consistent with chromia volatilization [26, 27] was generally observed for HK, TMA 4705, HP, and TMA 6301 from 650 to 750 °C (Figs. 1, 2, 3), (1,000 h at 650 °C, and 5,000 h at 700 and 750 °C). At 700 and 750 °C, the lower Cr/Ni CF8CP continued to show relatively lesser oxidation resistance consistent with a transition to Fe-oxide formation and spallation (CF8CP was not evaluated at 650 °C in air with 10 % H_2O). In contrast, the developmental alumina-forming alloy CAFA 4 generally showed excellent oxidation resistance and small positive mass gains (less than 1 mg/cm^2) from 700 to 800 °C for the 5,000 h test period.

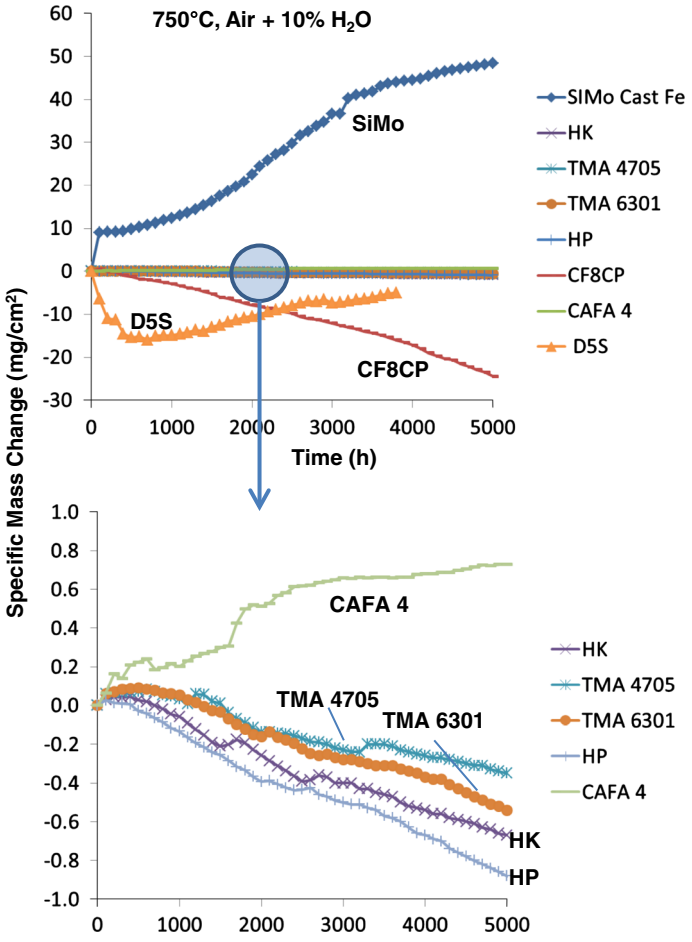

Fig. 3 Oxidation data (100 h cycles) at 750 °C in air with 10 % H_2O. Same data, two different specific mass change scales

(It should be noted that at 750 °C, the mass change data for CAFA 4 showed some irregular, small mass increases, with visual inspection of the CAFA 4 test coupon suggesting some local regions of more extensive oxidation that appeared to stabilize with longer oxidation times).

The potential for detrimental effects of water vapor on the oxidation resistance of chromia-formers is well established [14, 15]. As comparatively fewer oxidation studies of SiMo and D5S cast irons have been conducted in air versus air with water vapor, a simple dry air screening was conducted in the present work for qualitative comparative purposes of the relative extent of oxidation using two, 500 h cycles (Fig. 5). The mass changes at 650 and 700 °C for the SiMo were roughly comparable in both wet and dry conditions, with the dry air data falling within the relatively broad ~20 to 40 mg/cm^2 mass gain range observed with duplicate

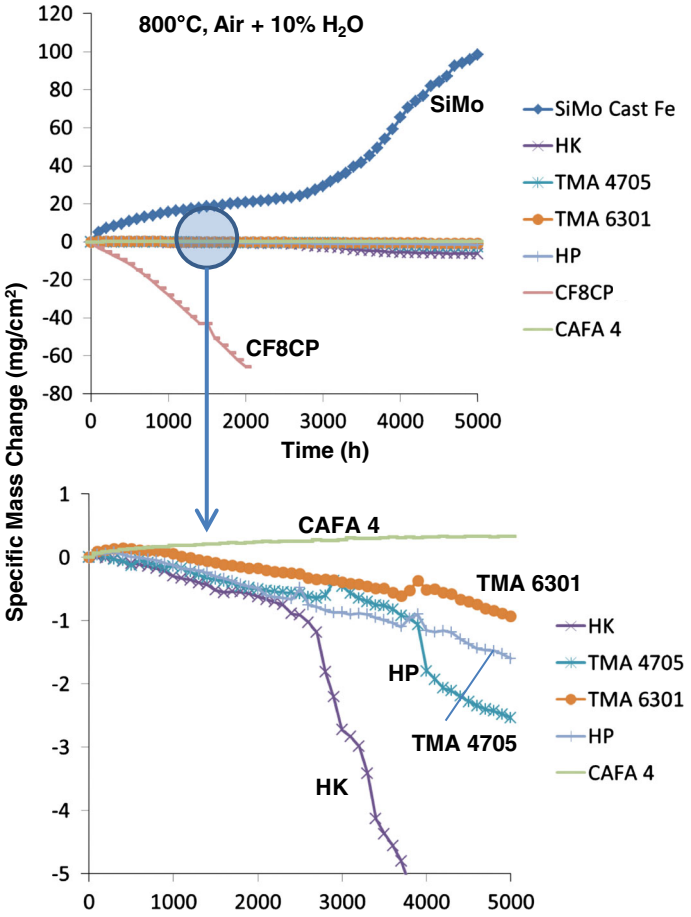

Fig. 4 Oxidation data (100 h cycles) at 800 °C in air with 10 % H_2O. Same data, two different specific mass change scales. The mass change data for CAFA 4, HP, and HK are from Ref. 24

samples after 1,000 h in air with 10 % water vapor (Fig. 5a). As with the wet air data, no significant spallation was observed for the SiMo in dry air.

For the D5S (Fig. 5b), very similar mass change data were observed at 650 °C under dry and wet conditions, with little spallation at this temperature. At 700 °C, significant spallation was observed for dry air exposed D5S, captured in the exposure crucible by the total sample + spall measurement mass change numbers shown in Fig. 5b. As previously presented, significant spallation was also observed for the 700 °C wet air D5S sample. (Similar total sample + spall mass change data was not obtained in wet air exposure, as crucibles with lids used in dry air exposure may limit access of the water vapor to the sample in wet air conditions). Overall, significant differences in the extent of oxidation at 650 and 700 °C in wet and dry air for the SiMo and D5S cast irons were not observed.

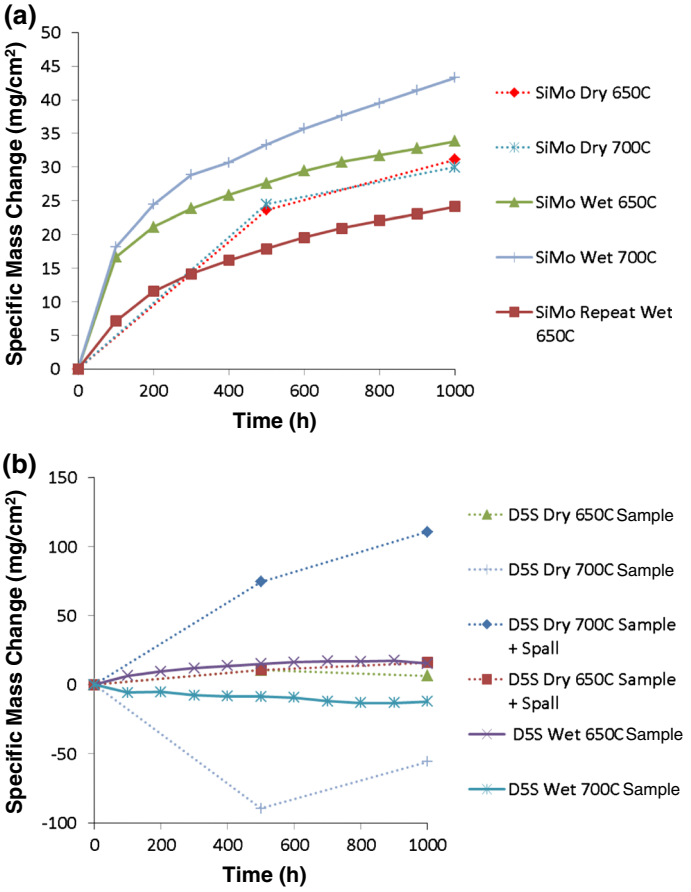

Fig. 5 Comparison of dry air oxidation data (500 h cycles) with wet air (air + 10 % H_2O) oxidation data for SiMo (**a**) and D5S (**b**) at 650 °C and 700 °C. The D5S 700 °C wet data in (**b**) is from a duplicate sample and is not the data from Fig. 2a

Oxidized Cross-Section Characterization

SiMo and D5S Cast Irons

The oxidized microstructure of D5S cast iron after 1,000 h of exposure at 650 and 700 °C in air with 10 % H_2O is shown in Fig. 6. At 650 °C, the total scale thickness was on the order of ~200–250 μm, approximately half of which was an external Fe-oxide scale (containing only trace Ni) and half a complex Fe–Ni–Si rich oxide subscale also containing some Cr and Mo (based on SEM/EDS analysis). (Characterization to distinguish if oxide subscale regions contained entrapped metal phases was not pursued). The external Fe-rich oxide scale contained many voids and continuous crack areas just above (~20 μm) and parallel to the scale-subscale interface (Fig. 6c). A similar external Fe-rich oxide scale + Fe–Ni–Si rich

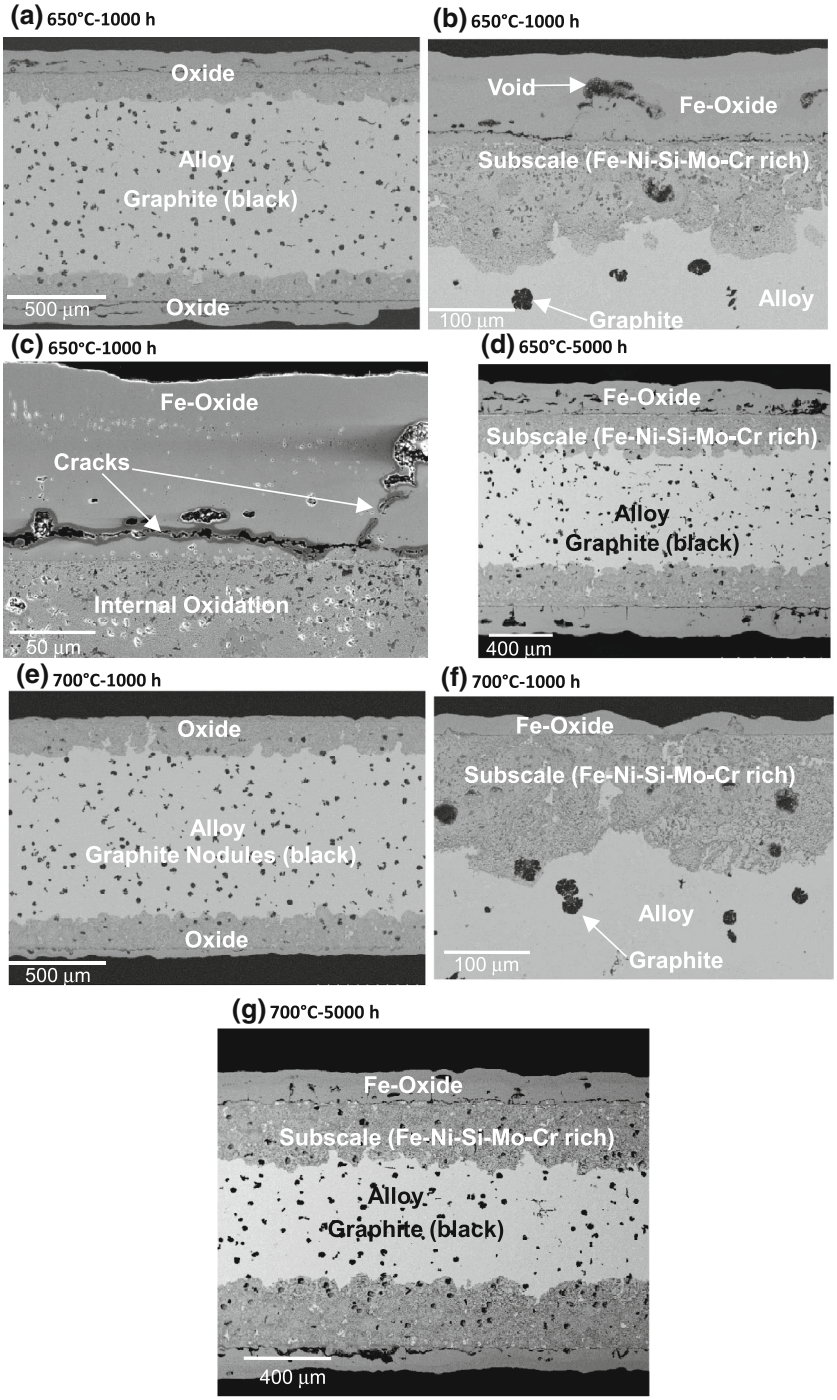
(a) 650°C-1000 h
Oxide
Alloy
Graphite (black)
500 µm
Oxide
(b) 650°C-1000 h
Void
Fe-Oxide
Subscale (Fe-Ni-Si-Mo-Cr rich)
100 µm
Graphite
Alloy
(c) 650°C-1000 h
Fe-Oxide
Cracks
Internal Oxidation
50 µm
(d) 650°C-5000 h
Fe-Oxide
Subscale (Fe-Ni-Si-Mo-Cr rich)
Alloy
Graphite (black)
400 µm
(e) 700°C-1000 h
Oxide
Alloy
Graphite Nodules (black)
Oxide
500 µm
(f) 700°C-1000 h
Fe-Oxide
Subscale (Fe-Ni-Si-Mo-Cr rich)
Alloy
100 µm
Graphite
(g) 700°C-5000 h
Fe-Oxide
Subscale (Fe-Ni-Si-Mo-Cr rich)
Alloy
Graphite (black)
400 µm

◀**Fig. 6** Backscatter SEM cross-section images of D5S cast iron after 1,000 h and 5,000 h in air with 10 % H_2O. **a–c** 650 °C/1,000 h; **d** 650 °C/5,000 h; **e**, **f** 700 °C/1,000 h; **g** 700 °C/5,000 h

oxide subscale was also observed after 1,000 h at 700 °C (Fig. 6e, f). However, the external Fe-rich oxide scale after 1,000 h was much thinner and irregular at 700 °C as a result of spallation (Fig. 2). It is likely that the oxide scale voids and cracking observed at 650 °C were more extensive at 700 °C, resulting in the spallation of much of the external Fe-oxide.

Despite the tendency for spallation by D5S at 700 °C, the 5,000 h external Fe-oxide scale and internal subscale cross-sections at 650 °C (Fig. 6d) and 700 °C (Fig. 6g) were similar, suggesting that the spallation at 700 °C primarily occurred during the first ~1,000 h of exposure, consistent with the mass change curves (Fig. 2) showing relative positive mass gains beyond 500–1,000 h. Graphite nodules from the underlying alloy microstructure were observed incorporated in the Fe–Ni–Si rich oxide subscale regions at both 650 and 700 °C, but not to any great extent in the external Fe-oxide regions. These observations are consistent with well-established understanding that the external Fe-oxide scale is outward growing and the internal subscale inward growing [e.g. 7–12].

Figure 7 shows the oxidized microstructure of SiMo cast iron after 1,000 h of exposure at 700 and 800 °C in air with 10 % H_2O. At 700 °C (Fig. 7a, b), the scale was duplex, consisting of an outer Fe-oxide layer on the order of 200 μm thick and an inner Fe–Si rich oxide layer also on the order of 200 μm thick. At the oxide-alloy interface, a 2–10 μm thick subscale region of internal Si rich oxidation products was observed (Fig. 7b). Graphite nodules from the underlying alloy microstructure were observed in the inner oxide layer. Voiding and some cracking were observed in the outer Fe-oxide region layer, with some of the voids appearing to blunt the connectivity of cracks. Overall, the microstructure pattern of graphite nodules in the oxidized regions indicates the inner Fe–Si oxide layer was inward growing and the outer Fe-oxide outward growing, similar to that observed or D5S and consistent with the literature [e.g. 7, 11, 12].

In contrast, after 1,000 h of exposure at 800 °C in air with 10 % H_2O, the SiMo cast iron formed an irregular but far thinner oxide scale (Fig. 7c, d), consistent with the mass change measurements which showed initially slower oxidation for the SiMo at 800 °C than 700 °C (Figs. 2, 4). The scale at 800 °C was again primarily duplex as was observed at 700 °C, but with an irregular outer Fe-oxide layer region and an inner Fe–Si rich oxide layer region of varying total scale thickness of 25–200 μm (regions of thinner scale and regions with thick Fe-oxide nodules). The key difference was the formation of a continuous Si-rich oxide layer, consistent with SiO_2 (identification based solely on EDS data), at the oxide-alloy interface at 800 °C, as opposed to internal oxidation of Si at 700 °C. The slower oxidation of SiMo at 800 versus 700 °C is attributed to this inner continuous SiO_2-base layer. Such behavior of a transition to SiO_2-rich oxide formation at the oxide-alloy interface with increasing temperature of oxidation was also reported by references [7, 11, 12].

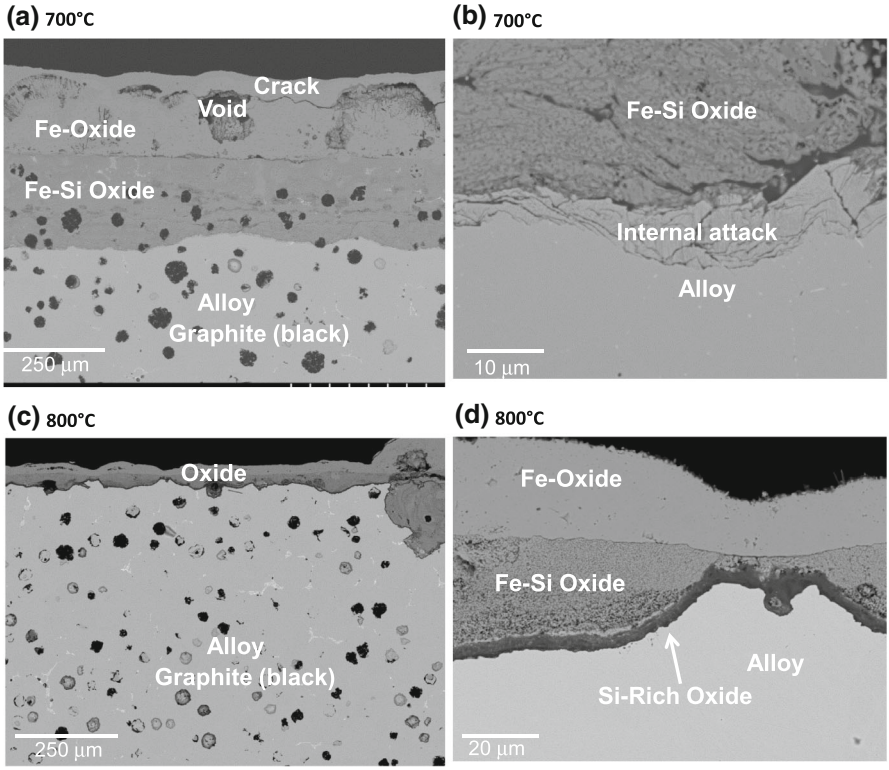

Fig. 7 Backscatter SEM cross-section images of SiMo cast iron after 1,000 h in air with 10 % H_2O. **a**, **b** 700 °C; **c**, **d** 800 °C

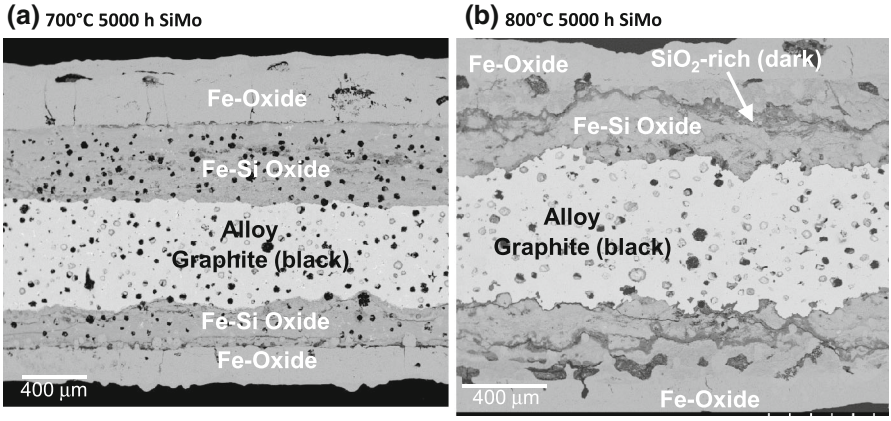

Fig. 8 Backscatter SEM cross-section images of SiMo cast iron after 5,000 h in air with 10 % H_2O. **a** SiMo 700 °C; **b** SiMo 800 °C

Figure 8 shows SEM cross-sections of SiMo cast iron after 5,000 h of exposure at 700 and 800 °C in air with 10 % H_2O. Continued oxidation at 800 °C beyond the 1,000 h cross-section shown in Fig. 7c, d resulted in breakdown of the continuous inner SiO_2 layer, which after 5,000 h can be observed as remnants within the middle of oxide scale, below which mixed Fe–Si rich oxide continued to form. This loss of protectiveness of the inner SiO_2 layer is consistent with the increased oxidation and mass uptake observed at around ~3,000 h of exposure at 800 °C (Fig. 4). The resultant oxide scale thickness and structure at 5,000 h is similar to that observed at 700 °C.

Cast Chromia- and Alumina-Forming Austenitics

In contrast to the thick oxide films formed on the SiMo and D5S cast irons, the chromia- and alumina-forming cast austenitics formed much thinner oxide scales. Figure 9a shows the oxidized cross-section of the 20Ni–25Cr class TMA 4705 alloy after 5,000 h at 800 °C in air with 10 % H_2O at the same magnification as shown in Fig. 8b for the similarly oxidized SiMo cast iron. Higher magnification cross-section images of TMA 4705 and HK, as well as the 35Ni–25Cr class TMA 6301 and HP, and alumina-forming CAFA 4 are shown in Fig. 9b–j. Oxide scale thickness after 5,000 h at 800 °C was on the order of ~25 μm for TMA 4705, HK, and HP (some areas of inhomogeneous oxide thickness suggest a degree of spallation likely occurred as well) and ~10 μm for the TMA 6301, and consisted primarily of mixed Cr_2O_3 and Fe–Cr rich oxides (based on SEM/EDS analysis). In addition to the external oxide scale formation, preferential internal attack along second phases at austenite matrix grain boundaries was observed in all the cast chromia-forming austenitics, extending an additional ~50 μm into the underlying alloy (qualitatively a little less internal attack for HK than the other alloys). These internal oxide attack regions in the cast, chromia-forming austenitics tended to be rich in Cr, Si, and/or Nb, based on qualitative screening by EDS. In contrast, the alumina-forming CAFA 4 alloy (Fig. 9i, j) generally showed oxide scale thickness in the micron range after 5,000 h at 800 °C, with occasional 5–10 μm Nb-rich surface nodules undercut by continuous alumina, typical of this class of alloys [28]. Only occasional local regions of minor internal attack (few microns) were observed in the CAFA 4 alloy.

EPMA Analysis of Select Cast Chromia Forming Austenitics

Because accelerated Cr depletion due to Cr oxy-hydroxide volatility of chromia-forming alloys in the presence of water vapor is a concern [e.g. 29], EPMA line scan analyses (1–2 μm steps) were conducted for the 19Cr–12Ni CF8CP, 25Cr–20Ni TMA 4705, and 25Cr–35Ni TMA 6301 alloys after 5,000 h at 700 and 800 °C in air with 10 % H_2O (Figs. 10, 11, 12). (Due to poor oxidation resistance and extensive scale spallation at 800 °C by the CF8CP, this alloy was examined after 2,000 h of exposure at 800 °C). The line scans were conducted for ~100 μm depth, beginning ~10 to 20 μm in the inner oxide scale moving through the oxide-alloy interface into the underlying alloy. The data tracked the levels of Cr, Fe, Mn, Mo, Ni, Nb, and

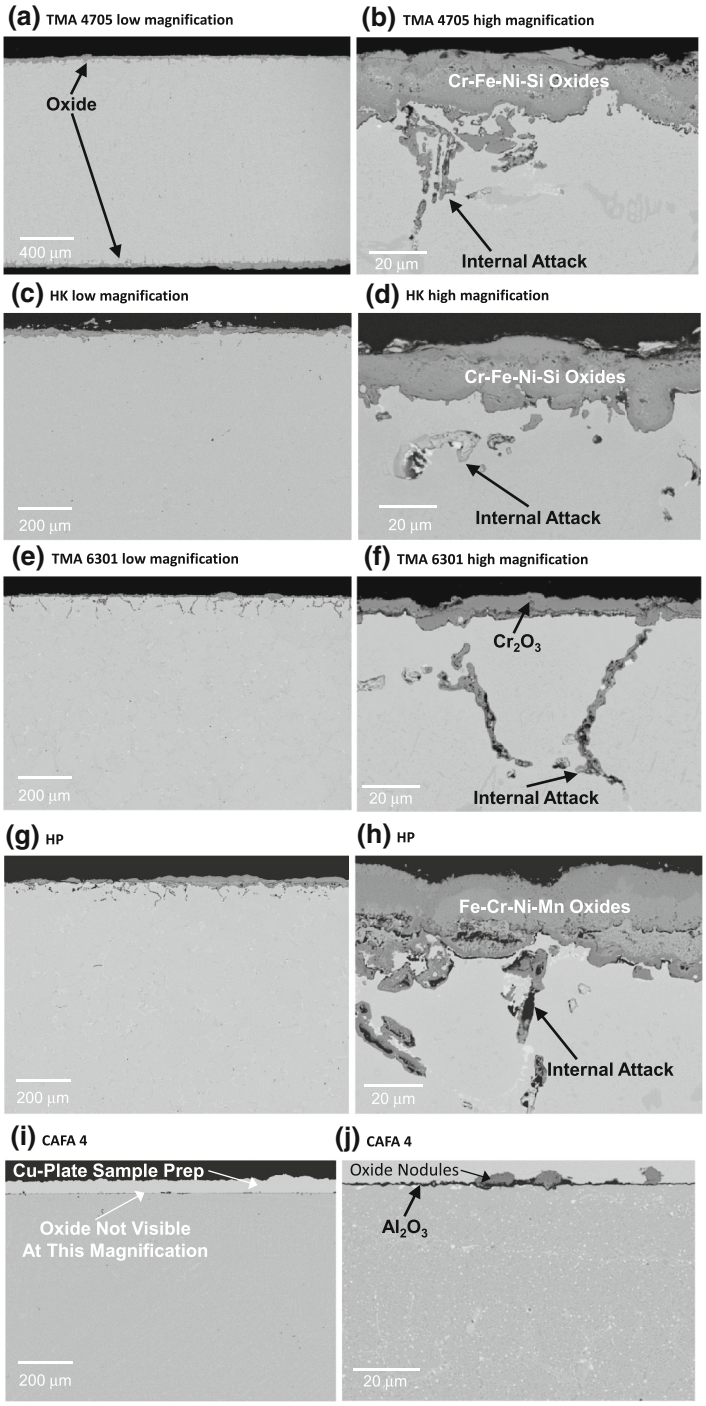
(a) TMA 4705 low magnification
Oxide
400 µm
(b) TMA 4705 high magnification
Cr-Fe-Ni-Si Oxides
20 µm
Internal Attack
(c) HK low magnification
200 µm
(d) HK high magnification
Cr-Fe-Ni-Si Oxides
20 µm
Internal Attack
(e) TMA 6301 low magnification
200 µm
(f) TMA 6301 high magnification
Cr_2O_3
20 µm
Internal Attack
(g) HP
200 µm
(h) HP
Fe-Cr-Ni-Mn Oxides
Internal Attack
20 µm
(i) CAFA 4
Cu-Plate Sample Prep
Oxide Not Visible
At This Magnification
200 µm
(j) CAFA 4
Oxide Nodules
Al_2O_3
20 µm

◀**Fig. 9** Backscatter SEM cross-section images of austenitic stainless steels after 5,000 h at 800 °C in air with 10 % H_2O. **a**, **b** TMA 4705; **c**, **d** HK; **e**, **f** TMA 6301; **g**, **h** HP; **i**, **j** CAFA 4

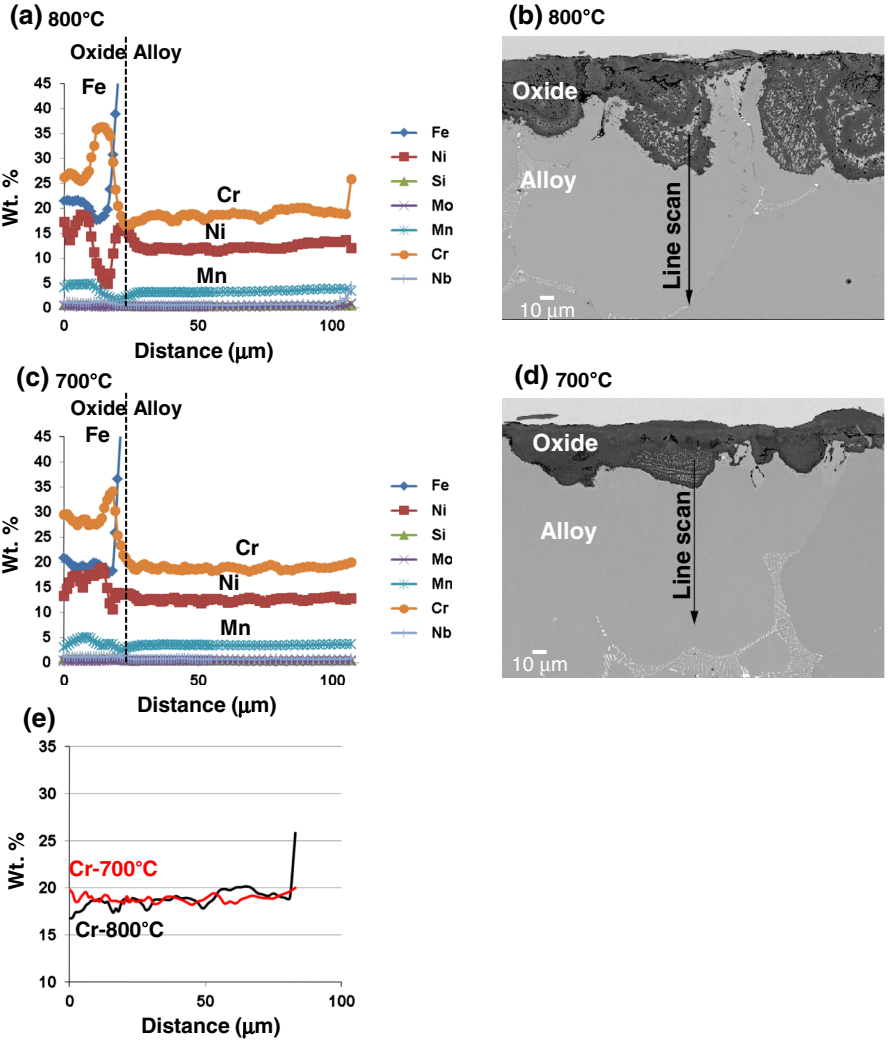

Fig. 10 EPMA line scan analysis for CF8CPN after 2,000 h at 800 °C in air with 10 % H_2O (**a**, **b**) and 5,000 h at 700 °C (**c**, **d**). Line scan data (**a**, **c**); SEM backscatter cross-section images of line scan locations (**b**, **d**); overlap plot of 700 and 800 °C Cr data (**e**)

Si. An estimate of the oxide-alloy interface is marked on the profile line scan data (Figs. 10, 11, 12a, c), based on the Fe profile and the total summation profile of all elements tracked (total summation not plotted in Figs. 10, 11, and 12).

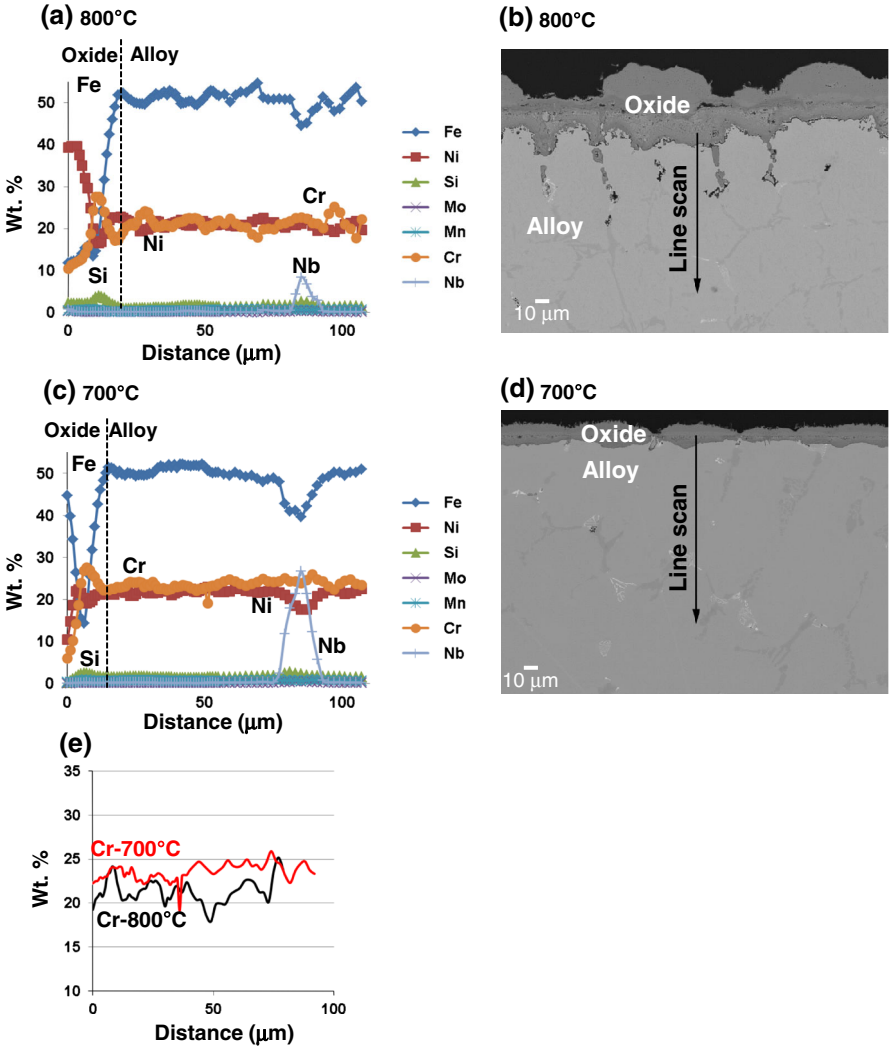

Fig. 11 EPMA line scan analysis for TMA 4705 after 5,000 h at 800 °C (**a**, **b**) and 700 °C in air with 10 % H_2O (**c**, **d**). Line scan data (**a**, **c**); SEM backscatter cross-section images of line scan locations (**b**, **d**); overlap plot of 800 and 700 °C Cr data (**e**)

At 800 °C, CF8CP formed extensive Fe–Ni–Cr–Mn rich oxide scale regions (Fig. 10a, c) extending tens to hundreds of microns into the underlying alloy (Fig. 10b) (Characterization to distinguish if oxide subscale regions contained entrapped metal phases was not pursued). A similar oxide structure was observed at 700 °C (Fig. 10d), although the total retained oxide scale thickness was generally less than 100 μm thick (note that scale spallation was observed at both temperatures, so scale cross-sections don't represent the full extent of oxidation). Such irregular, likely nodular-initiated attack is typical of the detrimental effects of

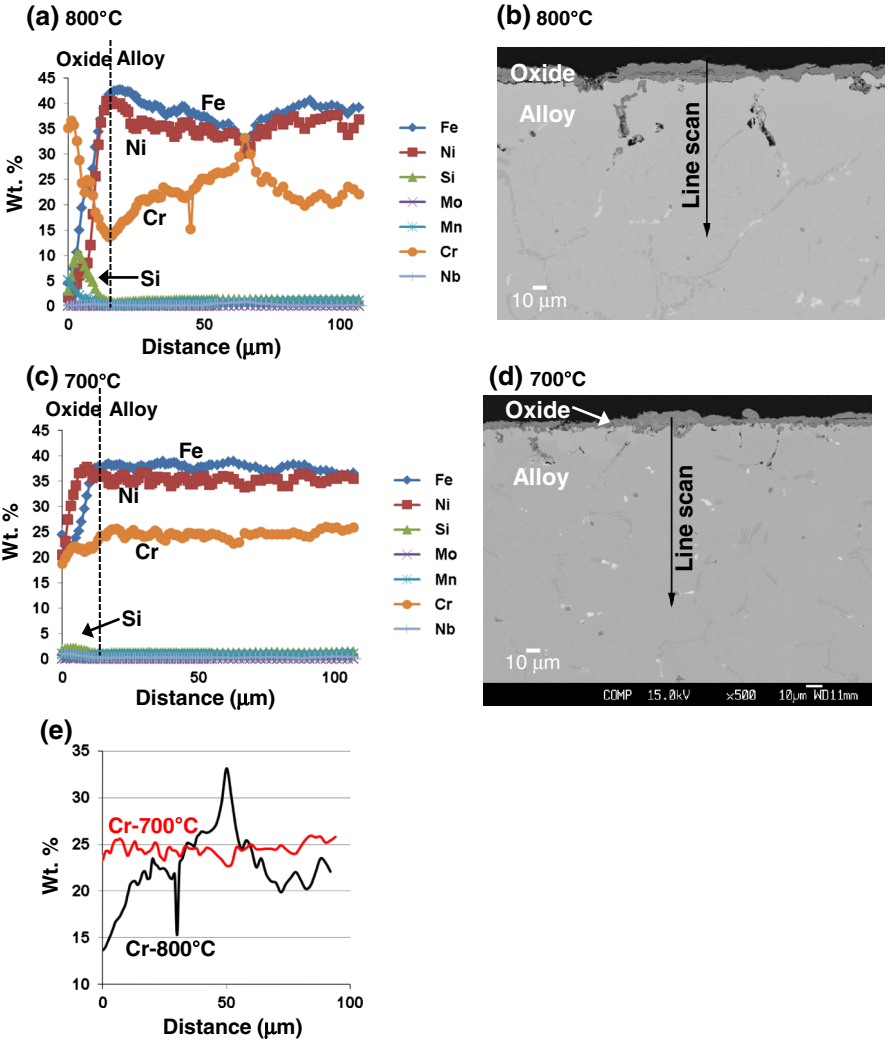

Fig. 12 EPMA line scan analysis for TMA 6301 after 5,000 h at 800 °C (**a**, **b**) and 700 °C in air with 10 % H_2O (**c**, **d**). Line scan data (**a**, **c**); SEM backscatter cross-section images of line scan locations (**b**, **d**); overlap plot of 800 and 700 °C Cr data (**e**)

water vapor on the oxidation resistance of chromia-forming alloys, resulting in a shift to more rapid Fe/Ni base metal oxidation. It has been attributed to depletion of Cr accelerated by Cr oxy-hydroxide volatility and/or enhanced internal oxidation by introduction of hydrogen from the water vapor into the alloy [15, 29–32]. The Cr line scans (Fig. 10e) showed little to no Cr depletion in the CF8CP 700 °C/5,000 h and 800 °C/2,000 h cross-sections. However, this may be a consequence of the extensive Fe–Ni–Cr rich oxide nodule formation consuming areas of Cr depletion, rather than strong evidence that Cr depletion did not occur [32]. The thickness of the

oxidation test coupons (1–1.5 mm thick) also provides a Cr reservoir for resupply of Cr. For example, Cr depletion in thin chromia-forming alloy foils (~0.1 mm thick) is exacerbated by lack of an alloy Cr reservoir for resupply [29].

Mixed Fe–Ni–Cr rich oxide scale regions were also observed for TMA 4705 at 5,000 h at 700 and 800 °C in air with 10 % H_2O (Fig. 11), although the extent of attack was significantly less than that for CF8CP (Figs. 2, 4, 10, 11). The Cr line scan profiles (Fig. 11e) suggested only modest Cr loss at 800 °C, and essentially none at 700 °C. In contrast, the 35Ni–25Cr TMA 6301 800 °C/5,000 h cross-section showed the greatest extent of Cr loss of the cross-sections analyzed (Fig. 12). The Cr level at the oxide-alloy interface at 800 °C in TMA 6301 decreased to 14–15 wt%, as opposed to 25 wt% in the bulk alloy. The Cr profile at 700 °C/5,000 h was essentially flat at around 25 wt% Cr. Based on the oxide scale thickness, lack of extensive oxide nodule formation, and mass change data, the TMA 6301 was the most oxidation resistant of the chromia-forming austenitics. The greater Cr depletion at 800 °C detected locally in TMA 6301 may be the result of its greater oxidation resistance; primarily thin chromia-base scale formation with little Fe–Ni–Cr oxide nodule formation that would consume the Cr depleted underlying alloy.

Discussion

The SiMo cast iron exhibited rapid oxidation and oxide scales hundreds of microns thick for the 1,000–5,000 h, 650–800 °C conditions studied in the present work. However, despite their great thickness and porosity, the oxide scales remained relatively adherent under the 100 h cycles studied and exhibited a degree of parabolic oxidation kinetics character (Figs. 1, 2, 3, 4). Given an estimated exhaust system hot lifetime of ~15,000 h (assumes 1 million mile engine lifetime with average peak cruise speed of 65 miles per hour), it is conceivable that SiMo cast irons may not be completely oxidation limited at the lower end of the 650–800 °C temperature range studied depending on the specifics of the design constraints, component thickness, and ability to tolerate metal section loss of hundreds of microns. Rather, hot strength and constrained thermal fatigue issues may play a more dominant role in determining the upper temperature use limit of the SiMo. An exception to this supposition is if oxide scale spallation becomes an issue during operation, as spalled oxide particles may result in downstream component damage. Such spallation is anticipated to be more prevalent for the shorter thermal cycles encountered in engine operation (<12 h) versus the relatively gentle 100 h cycles used in the present work to obtain long-term oxidation data.

The D5S type cast irons potentially offer marginally higher temperature capability from a hot strength and constrained thermal fatigue standpoint [33]. However, in the present work they showed increased susceptibility to oxide scale spallation at 700 and 750 °C, and thus may not offer significantly higher use temperatures than SiMo cast irons. Further, cross-sections of D5S and SiMo after 5,000 h at 700 °C in air with 10 % H_2O (Figs. 6g, 8a) showed a similar extent of attack. The high levels (~35 wt%) of Ni in D5S (Table 1) also result in

significantly higher cost than SiMo cast irons. The average coefficient of thermal expansion (CTE) for the D5S is essentially the same as for the SiMo cast iron, $\sim 12 \times 10^{-6}$ °C^{-1} [34, 35]. Spallation of such thick, complex oxide scale structures is a complex phenomenon, with interplay among CTE and thermomechanical behaviors and creep of both the oxide phases and underlying alloy substrate [e.g. 36]. For example, one speculated contributing factor for the spallation differences observed between SiMo and D5S may be that the greater creep strength of D5S (austenitic vs ferritic SiMo) may result in less strain accommodation of the thick, multi-layer oxide scales during thermal cycling, causing increased spallation. Further study is needed to better clarify the differences in spallation resistance observed for the SiMo and D5S in the present work.

The higher Cr/Ni chromia-forming austenitics exhibited generally good oxidation resistance over the course of the 5,000 h exposures studied. The presence of 10 vol% water vapor in the test environment resulted in degraded oxidation resistance by the 19Cr–12Ni CF8CP, with Fe-oxide nodule formation and extensive oxide scale spallation (this alloy class generally exhibits very good levels of oxidation resistance in dry air 650–800 °C conditions) [17, 18]. In contrast, the 20Ni–25Cr TMA 4705 and the 35Ni–25Cr HP and TMA 6301 alloys showed only minor volatility driven mass loss over the course of the 5,000 h exposure, and EPMA line scan analysis of the underlying alloy indicated that extensive Cr depletion was not present. This finding suggests that the oxidation resistance of these higher Cr/Ni alloys in water vapor may be maintained for far longer exposure periods than the 5,000 h studied. Of greater concern was the tendency toward internal oxidation along second phases (interdendritic phases typically are present in cast structures) and alloy grain boundaries in these cast chromia-forming alloys. Such attack can potentially result in degraded mechanical properties and in particular facilitate the initiation of fatigue cracks. From an oxidation standpoint, the CAFA 4 alloy offered the best overall oxidation resistance. The adoption of CAFA 4, or any of the chromia-forming advanced austenitics, in exhaust components will likely come down to castability and design considerations and if/how tradeoffs related to lower thermal conductivity and higher thermal expansion than cast irons ultimately affect monotonic and cyclic thermal stress generation during operation.

It is interesting to note that CF8CP was developed and commercialized in 2007 for use in a regeneration system housing exhaust component for the ceramic diesel particulate filters now required in the United States on all heavy-duty highway truck diesel engines [16]. This application involves rapid thermal cycling and peak temperatures reported to be >850 °C, with CF8CP exhibiting good oxidation resistance in this service application. This is in contrast to the relatively poor oxidation resistance observed for CF8CP in laboratory exposures at 700–800 °C in air with 10 % H_2O in the present work (Figs. 1, 2, 3, 4).

Possible reasons for this difference include lower levels of water vapor in the actual engine application than the 10 vol% H_2O level used in the present work. Diesel exhaust can contain $\sim$2–12 % H_2O range depending on a number of engine, fuel, and operation factors [13]. Chromia-formers such as CF8CP exhibit far better oxidation resistance in dry air than wet air [18], and lower levels of H_2O may be

expected to result in reduced oxidation rates. Other components in the exhaust gas may also result in a more reducing environment/lower pO_2 than air with 10 % H_2O used in the laboratory testing, which could also result in reduced oxidation rates under some circumstances. The actual truck service engine operation cycle may also result in lower effective metal time/temperature profiles than that suggested by the exhaust gas temperature, which may be effectively less severe from an oxidation standpoint than the 100 h cycles run in the laboratory work. The laboratory data does, however, provide a means to compare the oxidation resistance of the candidate alloys under well controlled conditions. Better understanding, comparison, and correlation between laboratory oxidation studies and operating engine environments are an area of significant future need.

From an oxidation mechanism standpoint, the oxide scale features of the SiMo and D5S cast irons were consistent with previous reports from short term (<500 h studies) in air and simulated exhaust gas environments [7–12]. Of particular interest for SiMo cast iron, Tholence and Norell [11] also observed continuous SiO_2 formation at the oxide–alloy interface for higher temperatures (850 °C), and discussed relative to theoretical and experimental work in the Fe–Si system for threshold of Si needed for external scale formation [37–40] whether at lower temperature of 650 °C a continuous inner SiO_2 layer will eventually develop. In the present work, continuous inner SiO_2 was not observed even after 5,000 h at 650 and 700 °C (Fig. 8a). Further at 800 °C, it was observed to form but not be maintained beyond ~3,000 h of exposure (Figs. 4, 7, 8). Therefore, a SiMo cast iron with low oxidation rates from SiO_2 formation for the desired 15,000 h hot lifetimes does not appear possible in the present composition ranges used (Table 1). The limited dry air screening data in the present work for the SiMo and D5S cast irons also suggests that 10 % H_2O did not result in significantly accelerated oxidation rates at 650 and 700 °C for these materials compared to air alone (Fig. 5).

Conclusions

The oxidation behavior of candidate cast alloys for diesel engine exhaust components was studied for up to 5,000 h at 650, 700, 750, and 800 °C in air with 10 % H_2O.

(1) The alloys in order of oxidation resistance from best to worse were: alumina-forming CAFA 4 > chromia-forming 35Ni–25Cr type TMA 6301 and HP > 25Ni–25Cr type TMA 4705 > 25Ni–25Cr type HK > 19Cr–12Ni CF8CP > SiMo and D5S.

(2) Oxide scale spallation issues were observed for D5S from 700 to 750 °C. SiMo exhibited moderately faster oxidation than D5S, but the scales remained relatively adherent despite reaching hundreds of microns in thickness under some conditions. These results suggest that D5S may not be a good alternative to SiMo to achieve higher operating temperatures in exhaust applications for designs where spalled oxide particles may damage downstream components.

(3) Accelerated oxidation in water vapor was observed for the 19Cr–12Ni CF8CP from 700 to 800 °C, with Fe-oxide formation and extensive scale spallation observed.
(4) Accelerated oxidation and/or water vapor volatility driven Cr loss was not a major issue for the 25Ni–25Cr chromia-forming austenitics up to 750 °C, and the 35Ni–25Cr chromia-forming austenitics up to 800 °C (highest temperature studied). These alloys exhibited good oxidation behavior out to the 5,000 h test duration studied, with EPMA line scans of Cr levels near the oxide–alloy interface suggesting that the good oxidation resistance may be maintained for longer periods. A concern for this class of alloys was internal attack of second phases at alloy austenitic matrix grain boundaries, which may lead to degradation in strength and/or thermal fatigue characteristics.
(5) The developmental family of cast alumina-forming austenitic steels offer potential for improved oxidation resistance in exhaust environments. Their adoption (as well as the potential adoption of chromia-forming austenitics) will depend on their weldability, castability and exhaust system design suitability, particularly with regards to thermal conductivity and expansion properties that determine the thermal fatigue resistance in service.

Acknowledgments The authors thank Duraloy Technologies, Inc. for providing cast austenitic stainless steels TMA 4705, TMA 6301, HP, and HK materials for study. T. Lowe, M. Stephens, G. Garner, and T. Jordan are thanked for experimental work and A. Shyam, S. Dryepondt, and B Pint for helpful comments on this manuscript. Research sponsored by the U.S. Department of Energy, Office of Energy Efficiency and Renewable Energy, Vehicle Technologies Office, Propulsion Materials Program (managed by J. Gibbs).

References

1. D. Li and C. Sloss, Ferrous high-temperature alloys for exhaust component applications. *SAE International Journal of Material and Manufacturing* **3**, (1), 391–404 (2010).
2. D. Li, C. Sloss and S. Amer Foundry, Cast ferritic stainless steels for automotive exhaust components. *Transactions of the American Foundry Society* **121**, 487–494 (2013).
3. K. Dawi, J. Favergeon, and G. Moulin, High temperature corrosion of the Si-Mo cast iron in exhaust atmosphere. *High Temperature Corrosion and Protection of Materials* **7**, Pts 1 and 2 595–598, 743–751 (2008).
4. Y. J. Kim, H. Jang and Y. J. Oh, High-temperature low-cycle fatigue property of heat-resistant ductile-cast irons. *Metallurgical and Materials Transactions A-Physical Metallurgy and Materials Science* **40A**, (9), 2087–2097 (2009).
5. Y. L. Yang, Z. Y. Cao, Y. Qi, and Y. B. Liu, The study on oxidation resistance properties of ductile cast irons for exhaust manifold at high temperatures, in *Manufacturing Science and Engineering*, Pts 1–5, vol. 97–101. *Advanced Materials Research,* eds. Z. Jiang, and C. L. Zhang (Trans Tech Publications, Switzerland, 2010), pp. 530–533.
6. K. H. Choe, S. M. Lee and K. W. Lee, High temperature oxidation behavior of Si-Mo ferritic ductile cast iron. *Materials Science Forum* **654–656**, 542–545 (2010).
7. M. Ekstrom, P. Szakalos and S. Jonsson, Influence of Cr and Ni on high-temperature corrosion behavior of ferritic ductile cast iron in air and exhaust gases. *Oxidation of Metals* **80**, (5–6), 455–466 (2013).

8. F. Tholence and M. Norell, High temperature corrosion of cast irons and cast steels in dry air, in *High Temperature Corrosion and Protection of Materials 5*, eds. by R. Streiff, I. G. Wright, R. C. Krutenat, M. Caillet, A. Galerie, Pts 1 and 2, vol. 369–373. *Materials Science Forum*, (Trans Tech Publications, Switzerland, 2001), pp. 197–204.
9. F. Tholence and M. Norell, AES characterization of oxide grains formed on ductile cast irons in exhaust environments. *Surface and Interface Analysis* **34**, (1), 535–539 (2002).
10. F. Tholence and M. Norell, Nitride precipitation during high temperature corrosion of ductile cast irons in synthetic exhaust gases. *Journal of Physics and Chemistry of Solids* **66**, (2–4), 530–534 (2005).
11. F. Tholence and M. Norell, High temperature corrosion of cast alloys in exhaust environments I-ductile cast irons. *Oxidation of Metals* **69**, (1–2), 13–36 (2008).
12. F. Tholence and M. Norell, High temperature corrosion of cast alloys in exhaust environments. II-Cast stainless steels. *Oxidation of Metals* **69**, (1–2), 37–62 (2008).
13. J. B. Heywood, *Internal Combustion Engines Fundamentals*. McGraw-Hill Mechanical Engineering. ISBN: 9780070286375 (1988).
14. S. R. J. Saunders, M. Monteiro and F. Rizzo, The oxidation behaviour of metals and alloys at high temperatures in atmospheres containing water vapour: a review. *Progress in Materials Science* **53**, (5), 775–837 (2008).
15. W. J. Quadakkers, J. Zurek and M. Hansel, Effect of water vapor on high-temperature oxidation of FeCr alloys. *Journal of the Minerals Metals and Materials Society* **61**, (7), 44–50 (2009).
16. P. J. Maziasz, P. J. Shingledecker, N. D. Evans and M. J. Pollard, Developing new cast austenitic stainless steels with improved high-temperature creep resistance. *Journal of Pressure Vessel Technology* **131**, 051404 (2009).
17. P. J. Maziasz and B. A. Pint, High-temperature performance of cast CF8C-plus austenitic stainless steel. *Journal of Engineering for Gas Turbines and Power-Transactions of the ASME* **133**, (9), 092102 (2011).
18. J. A. Haynes, B. L. Armstrong, D. Kumar, S. Dryepondt and Y. Zhang, Oxidation of slurry aluminide coatings on cast stainless steel alloy CF8C-plus at 800 A degrees C in water vapor. *Oxidation of Metals* **80**, (3–4), 363–387 (2013).
19. R. I. Pankiw, G. Muralidharan, and V. K. Sikka, Development of stronger and more reliable cast austenitic stainless steels (H-series) based on scientific and design methodology 2006-06-30, OSTI ID: 886136, ORNL/TM-2006/45 (2006).
20. R. I. Pankiw, G. Muralidharan, V. K. Sikka, and P. J. Maziasz, Cast heat-resistant austenitic steel with improved temperature creep properties and balanced alloying element additions and methodology for development of the same, US patent 8,318,083 (Nov 27, 2012).
21. G. Muralidharan, V. K. Sikka, P. J. Maziasz, and R. I. Pankiw, Cast, heat-resistant austenitic stainless steels having reduced alloying element content, US Patent US 7,749,432 (Jul 6, 2010).
22. G. Muralidharan, V. K. Sikka, P. J. Maziasz, and R. I. Pankiw, Cast, heat-resistant austenitic stainless steels having reduced alloying element content, US Patent 8,003,045 (Aug 23, 2011).
23. G. Muralidharan, Y. Yamamoto, and M. P. Brady, Cast alumina forming austenitic stainless steels. US Patent 8,431,072 (April 30, 2013).
24. G. Muralidharan, Y. Yamamoto, and M. P. Brady, submitted.
25. B. A. Pint, J. P. Shingledecker, M. P. Brady, and P. J. Maziasz, Proceedings of GT2007 ASME Turbo Expo 2007: Power for Land, Sea, and Air May 14–17 (Montreal, Canada, 2007), 3, 995–1002 (2007).
26. E. J. Opila, Volatility of common protective oxides in high-temperature water vapor: Current understanding and unanswered questions, in *High Temperature Corrosion and Protection of Materials* 6, Prt 1 and 2, Proceedings, vol. 461–464. *Materials Science Forum*, eds. P. Steinmetz, I. G. Wright, G. Meier, A. Galerie, B. Pieraggi, and R. Podor (2004).
27. H. Asteman, J. E. Svensson, L. G. Johansson and M. Norell, Indication of chromium oxide hydroxide evaporation during oxidation of 304 L at 873 K in the presence of 10 % water vapor. *Oxidation of Metals* **52**, (1–2), 95–111 (1999).
28. M. P. Brady, Y. Yamamoto, M. Santella and L. Walker, Composition, microstructure, and water vapor effects on internal/external oxidation of alumina-forming austenitic stainless steels. *Oxidation of Metals* **72**, (5–6), 311–333 (2009).
29. D. J. Young and B. A. Pint, Chromium volatilization rates from Cr_2O_3 scales into flowing gases containing water vapor. *Oxidation of Metals* **66**, (3–4), 137–153 (2006).
30. E. Essuman, G. H. Meier, J. Zurek, M. Hansel and W. J. Quadakkers, The effect of water vapor on selective oxidation of Fe–Cr alloys. *Oxidation of Metals* **69**, (3–4), 143–162 (2008).

31. E. Essuman, G. H. Meier, J. Zurek, M. Hansel, L. Singheiser and W. J. Quadakkers, Enhanced internal oxidation as trigger for breakaway oxidation of Fe–Cr alloys in gases containing water vapor. *Scripta Materialia* **57**, (9), 845–848 (2007).
32. R. Peraldi and B. A. Pint, Effect of Cr and Ni contents on the oxidation behavior of ferritic and austenitic model alloys in air with water vapor. *Oxidation of Metals* **61**, (5–6), 463–483 (2004).
33. A. Shyam, S. Hawkins, D. Erdman, R. England and G. Muralidharan, Constrained thermal fatigue performance of several cast ferrous alloys. *Materials Science Forum* **783–786**, 2388–2393 (2014).
34. R. Covert, J. Morrison, and K. Rohrig, Properties and applications of Ni-resist and ductile Ni-resist alloys. Publisher: Nickel Development Institute (1998) http://www.nickelinstitute.org/~/Media/Files/TechnicalLiterature/PropertiesandApplicationsofNi_ResistandDuctileNi_ResistAlloys_11018_.pdf.
35. F. Cverna, *Thermal Expansion ASM Ready Reference: Thermal Properties of Metals*, (ASM International, Materials Park, 2002).
36. A. S. Sabau and I. G. Wright, Influence of oxide growth and metal creep on strain development in the steam-side oxide in boiler tubes. *Oxidation of Metals* **73**, 467–492 (2010).
37. A. Atkinson, A theoretical-analysis of the oxidation of Fe–Si alloys. *Corrosion Science* **22**, (2), 87–102 (1982).
38. F. Gesmundo and F. Viani, Transition from internal to external oxidation for binary alloys in the presence of an outer scale. *Oxidation of Metals* **25**, 269–282 (1986).
39. R. C. Logani and W. W. Smeltzer, Development Of the wustite-fayalite scale on an iron-1.5 wt percent silicon alloy at 1000 degrees C. *Oxidation of Metals* **3**, (1), 15 (1971).
40. I. Svedung and Ng Vannerbe, Influence of silicon on oxidation properties of iron. *Corrosion Science* **14**, (6), 391 (1974).